PLY THICKNESS INFLUENCE IN IMPACT DAMAGE ON CAI CARBON/EPOXY TEST SPECIMENS

Thiago H. L. Pinto[1], Carlos A. Cimini Jr.[2], Sung K. Ha[3], Pedro H. Cabral[4], Gustavo H. C. Silva[4] and Alex P. Prado[4]

[1]Universidade Federal dos Vales do Jequitinhonha e Mucuri, UFVJM, Rodovia MGT 367, km 583, 5000, Alto da Jacuba, Diamantina, 39100-000, MG, Brazil, thiago.lara@ict.ufvjm.edu.br
[2]Universidade Federal de Minas Gerais, UFMG, Av. Antônio Carlos 6627, Belo Horizonte, 31270-901, MG, Brazil, cimini@ufmg.br
[3]Hanyang University, 222 Wangsimni-ro, Sageun-dong, Seongdong-gu, Seoul, South Korea, sungkha@gmail.com
[4]Embraer S.A., Av. Brigadeiro Faria Lima, 2.170, São José dos Campos, 12227-901, SP, Brazil, pedro.cabral@embraer.com.br, gustavo.caprio@embraer.com.br, alex.prado@embraer.com.br

Keywords: Composite plates, Compression after impact (CAI) test specimens, Finite elements, Ply thickness, Ply arrangement

ABSTRACT

Damage generated due to low velocity impact in carbon/epoxy thick and thin ply composite laminates is evaluated. Hashin failure criterion was used. Both thick and thin ply models have standard CAI test specimen dimensions, with same thickness and different ply number. Thick-to-thin ply thickness ratio was assumed to be 4. Quasi-isotropic and cross-ply layups were considered, with eight plies for the thick ply model, respectively stacked as $[+45/0/–45/90]_S$ and $[0/90]_{2S}$, and thirty-two plies for the thin ply model, respectively stacked as $[+45/0/–45/90]_{4S}$ and $[0/90]_{8S}$. A low velocity impact of a rigid sphere, using iced water density in order to simulate hail was replicated in both models, with sufficient energy to generate damage with no perforation. The goal of this work is to fully understand the possible benefits offered by different ply thickness in composite materials, being possible to observe a tendency of greater local stiffness and less damage for thin laminates.

1 INTRODUCTION

Advanced composite materials are widely used in the aerospace industry due to its high stiffness and strength-to-weight ratio and inherent anisotropy, which provides elastic and mass tailoring abilities for structural component design. However, complex and costly test programs are necessary to fully characterize the material and the failure modes. In recent years, significant effort has been made to develop accurate numerical methods, which would help in offsetting this cost.

Impact damage generated in composite laminates has been a topic of interest for researchers for a long time. In the last couple of decades, experimental and simulation results have been extensively conducted and published. This includes review papers on the state-of-the-art of the subject, such as Cantwell and Morton [1], Richardson and Wisheart [2], and Elde [3]. Moreover, both bi-dimensional [4][5][6] and three-dimensional simulations [7], delamination models [8][9][10], impact dynamics [11][12], and use of cohesive hypothesis [13][14], have also been studied. However, the damage generated due to an impact on thin ply laminates is not sufficiently explored, although thin ply composites have been around for a while.

The aim of this study is to evaluate the effects of damage generated due to low velocity impact in carbon/epoxy thick and thin ply composite laminates. The study presents simulation results for the impact damage generated in the laminates so that further predictions can be made for after impact loading schemes, such as compression after impact (CAI), tension after impact (TAI), and shear after impact (ShAI).

2 METHODOLOGY

The influence of thick versus thin ply composite laminates was evaluated using the Hashin failure criterion. Both thick and thin ply models have standard CAI test specimen dimensions [15], with same thickness and different ply number. Quasi-isotropic and cross-ply layups were considered, with eight plies for the thick ply model, disposed as $[+45/0/–45/90]_S$ and $[0/90]_{2S}$ respectively for each case, and thirty-two plies for the thin ply model, disposed as $[+45/0/–45/90]_{4S}$ and $[0/90]_{8S}$ respectively for each case.

Most composite materials are reinforced with strong and stiff fibers, if compared with it's matrix portion, leading to a clear distinction between fiber and inter-fiber (matrix, interface) failure modes. Those characteristics allows a failure a simplified and more physically significant failure treatment in the case of maximum stress, maximum strain and fully interactive theories [16]. The Hashin failure criterion [17] was used in this work for ply failure.

2.1 Hashin Failure Criteria

Hashin damage initiation criteria is applied in order to model anisotropic damage in fiber-reinforced materials. The response of the undamaged material is assumed to be linearly elastic, and the model is intended to predict behaviour of fiber-reinforced materials for which damage can be initiated without a large amount of plastic deformation. The Hashin's initiation criteria are used to predict the onset of damage, and the damage evolution law is based on the energy dissipated during the damage process and linear material softening [17].

Four different modes of failure are considered: fiber rupture in tension; fiber buckling and kinking in compression; matrix cracking under transverse tension and shearing; and matrix crushing under transverse compression and shearing [17].

- Fiber tension ($\sigma_{11} > 0$):

$$F_f^T = \left(\frac{\sigma_{11}}{X^T}\right)^2 + \alpha \cdot \left(\frac{\sigma_{12}}{S^L}\right)^2 \quad \text{where } 0 \le \alpha \le 1 \tag{1}$$

- Fiber compression ($\sigma_{11} < 0$):

$$F_f^C = \left(\frac{\sigma_{11}}{X^C}\right)^2 \tag{2}$$

- Matrix tension ($\sigma_{22} > 0$):

$$F_m^T = \left(\frac{\sigma_{22}}{Y^T}\right)^2 + \left(\frac{\sigma_{12}}{S^L}\right)^2 \tag{3}$$

- Matrix compression ($\sigma_{22} < 0$):

$$F_m^C = \left(\frac{\sigma_{22}}{2S^T}\right)^2 + \left[\left(\frac{Y^C}{2S^T}\right)^2 - 1\right] \cdot \frac{\sigma_{22}}{Y^C} + \left(\frac{\sigma_{12}}{S^L}\right)^2 \tag{4}$$

In the above equations, X^T denotes the longitudinal tensile strength, X^C denotes the longitudinal compressive strength; Y^T denotes the transverse tensile strength; Y^C denotes the transverse compressive strength; S^L denotes the longitudinal shear strength; S^T denotes the transverse shear strength; α is a coefficient that determines shear stress contribution to the fiber initiation criterion; and σ represents the

effective stress, with its components intended to represent the stress acting over the damaged area that effectively resists the internal forces.

The initiation criteria presented above can be specialized to obtain the model proposed in Hashin and Rotem in 1973 [18] by setting $\alpha = 0$ and $S^T = Y^C/2$, or the model proposed in Hashin in 1980 by setting $\alpha = 1$ [17]. An output variable is associated with each initiation criterion (fiber tension, fiber compression, matrix tension, and matrix compression) to indicate whether the criterion has been met. A value of 1.0 or higher indicates that the initiation criterion has been met [17].

These criteria were originally developed for unidirectional composites, as in the aforementioned configuration, and hence, implemented within two dimensional classical lamination approach for point stress calculations with ply discounting as the material degradation model. Failure indices for Hashin criteria are related to fiber and matrix failures and involve four failure modes. The criteria are extended to three dimensional problems where the maximum stress criteria are used for transverse normal stress component. The failure modes included in Hashin's criteria are as follows [17].

- Tensile fibre failure ($\sigma_{11} > 0$):

$$\left(\frac{\sigma_{11}}{X_T}\right)^2 + \frac{\sigma_{12}^2 + \sigma_{13}^2}{S_{12}^2} \tag{5}$$

- Compressive fibre failure ($\sigma_{11} < 0$):

$$\left(\frac{\sigma_{11}}{X_C}\right)^2 \tag{6}$$

- Tensile matrix failure for ($\sigma_{22} + \sigma_{33} > 0$):

$$\frac{(\sigma_{22} + \sigma_{33})^2}{Y_T^2} + \frac{\sigma_{23}^2 - \sigma_{22}\sigma_{33}}{S_{23}^2} + \frac{\sigma_{12}^2 + \sigma_{13}^2}{S_{12}^2} \tag{7}$$

- Compressive matrix failure ($\sigma_{22} + \sigma_{33} < 0$):

$$\left[\left(\frac{Y_C}{2S_{23}}\right)^2 - 1\right]\left(\frac{\sigma_{22} + \sigma_{33}}{Y_C}\right) + \frac{(\sigma_{22} + \sigma_{33})^2}{4S_{23}^2} + \frac{\sigma_{23}^2 - \sigma_{22}\sigma_{33}}{S_{23}^2} + \frac{\sigma_{12}^2 + \sigma_{13}^2}{S_{12}^2} \tag{8}$$

- Interlaminar tensile failure ($\sigma_{33} > 0$):

$$\left(\frac{\sigma_{33}}{Z_T}\right)^2 \tag{9}$$

- Interlaminar compression failure ($\sigma_{33} < 0$):

$$\left(\frac{\sigma_{33}}{Z_C}\right)^2 \tag{10}$$

where, σ_{ij} denote the stress components; subscripts *T* and *C,* the tensile and compressive allowable strengths for lamina, respectively. X_T, Y_T, Z_T denotes the allowable tensile strengths in three respective material directions. X_C, Y_C, Z_C, the allowable tensile strengths in three respective material directions. Further, S_{12}, S_{13} and S_{23} denote allowable shear strengths in the respective principal material directions.

3 ANALYSIS AND RESULTS

In order to verify model's mesh and configuration dependency, different arrangements are shown below. A unidirectional carbon/epoxy material is defined to each lamina, using the elastic properties shown in Table 1 [16].

Table 1 - Elastic properties of the unidirectional carbon/epoxy ply [16]

E_{11} $[MPa]$	E_{22} $[MPa]$	E_{33} $[MPa]$	ν_{12}	ν_{13}	ν_{23}	G_{12} $[MPa]$	G_{13} $[MPa]$	G_{23} $[MPa]$
164000	12000	12000	0.32	0.32	0.45	4500	4500	2500

The allowable strength values adopted in this work are presented in Table 2 [16].

Table 2 - Allowable stresses of the unidirectional carbon/epoxy ply [16]

X_1^t $[MPa]$	X_1^c $[MPa]$	X_2^t $[MPa]$	X_2^c $[MPa]$	X_3^t $[MPa]$	X_3^c $[MPa]$
2724	1690	50	111	290	290

The shear strength of the unidirectional carbon/epoxy ply presented is shown in Table 3

Table 3 – Shear strength of the unidirectional carbon/epoxy ply [16]

S_{12} $[MPa]$	S_{13} $[MPa]$	S_{23} $[MPa]$
120	137	90

The following subsections presents the convergence and impact energy studies, followed by results of two model configurations: First, cross-ply layups results were presented, with eight plies for the thick ply model $[0/90]_{2S}$ and thirty-two plies for the thin ply model $[0/90]_{8S}$, followed by quasi-isotropic layups results, with eight plies for the thick ply model $[+45/0/–45/90]_S$ and thirty-two plies for the thin ply model $[+45/0/–45/90]_{4S}$. Both thick and thin ply models have standard CAI test specimen dimensions [15], with same thickness and different ply number.

For computational time reduction proposes, the model presented in the cross-ply results is a model with two symmetry planes, only a quarter of the plate is shown in the figure 1 (right). The planes of symmetry are placed in top and left borders, the impact point being the upper left end, and the support constraints applied to the bottom and right. Due to the quasi-isotropic layups characteristics, the planes of symmetry, XZ and YZ, are not functional and, for quasi-isotropic analyses, the complete model (figure 1 left) were used. Besides this simplification, the results shown in section 3.3 are presented in complete domain, so mirroring the cross-ply results in both symmetry planes.

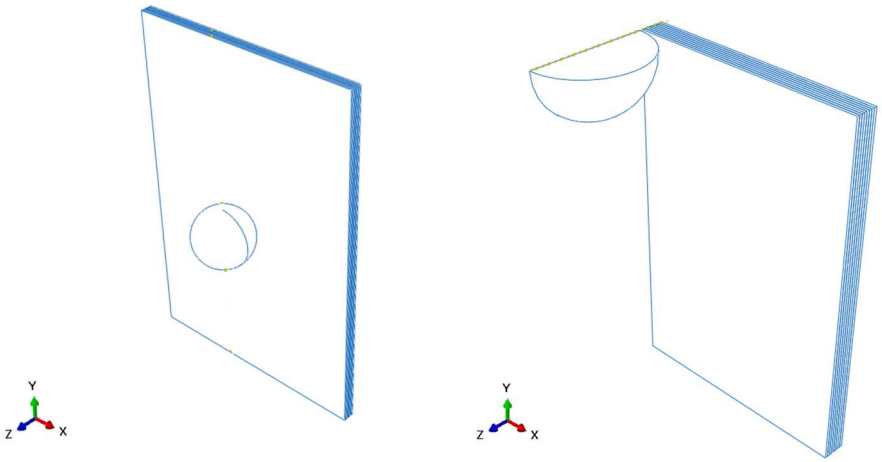

Figure 1 – Representation of complete model (left) and simplified model where two planes of symmetry were applied (right).

3.1 Mesh Dependency Studies

Three-dimensional model meshes with totals of 4,800, 8,960, 14,144, 25,760, 29,600 and 35,424 hexahedral elements were developed. However, thick and thin ply meshes differ in the number of nodes due to their different number of inter-ply sections. A low velocity impact of a rigid sphere was simulated in both models of each element number configuration, with sufficient energy to generate damage with no perforation, in order to verify the mesh influence in the results.

Figure 2 shows the maximum value for the most critical ("matrix" tensile transverse) damage generated for thick ply laminates during the impact and the percentage error if compared with the value of the model with fewer elements. The error, calculated comparing the current value with the obtained by the next coarser mesh result, shows a reduction as the mesh is refined.

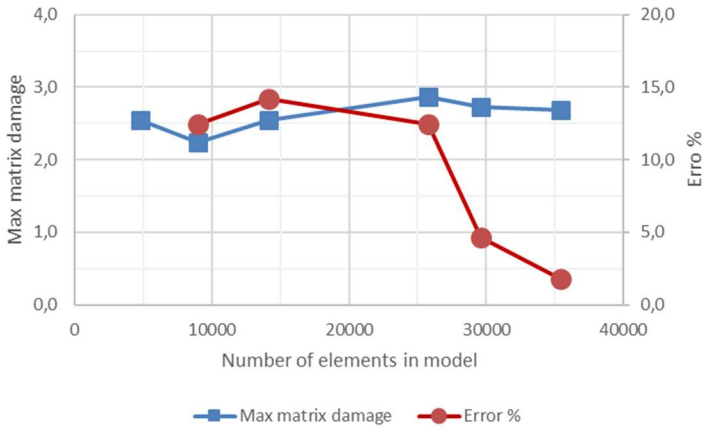

Figure 2 – Maximum value for the most critical ("matrix" tensile transverse) damage generated and percentage error for each mesh configuration.

Figure 3 shows comparisons for the damage generated for thick ply laminates during the impact. It can be seen that the impact behavior of the four models reveals mesh dependency, tending this dependence to be reduced as the mesh is refined.

The models presented herein were developed in ABAQUS. The mesh analysis and selection was limited by the computational consumed analyses time. However, the mesh convergence study reveals mesh dependency, as shown above, the behavior when changing the arrangement of layers is maintained.

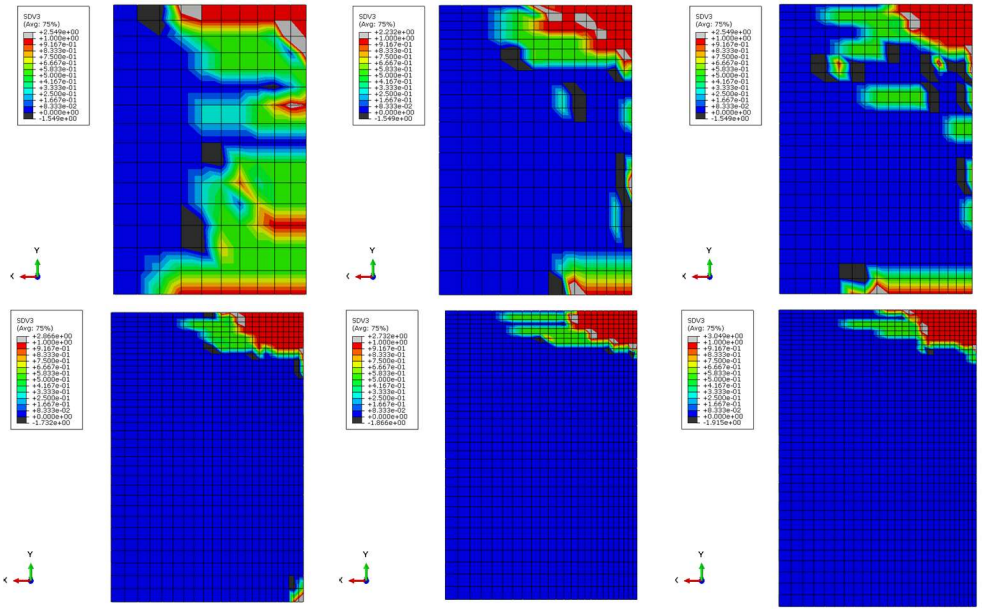

Figure 3 – Tensile transverse damage generated in bottom layer for each mesh. From left to right in the top row: 4,800, 8,960, 14,144; and in the bottom row: 25,760, 29,600 and 35,424 hexahedral elements.

3.2 Impact Energy Studies

Adopting the three-dimensional model mesh with a total of 35,424 hexahedral elements impact of a 1 inch "iced water" sphere, in order to simulate a hail impact, was simulated in order to verify the range of velocities with sufficient energy to generate damage with no perforation.

Figure 4 shows comparisons for the behavior of thick ply laminates during the impact, using initial velocities of 95 km/h, 227 km/h and 550 km/h in order to simulate energies of 3 J, 17 J and 100J, respectively. For 3 J and 17 J cases, besides the damage, no complete perforation occurs. It's possible to observe a high damage with complete perforation for 100 J energy impact, being this case excluded from the scope of this work.

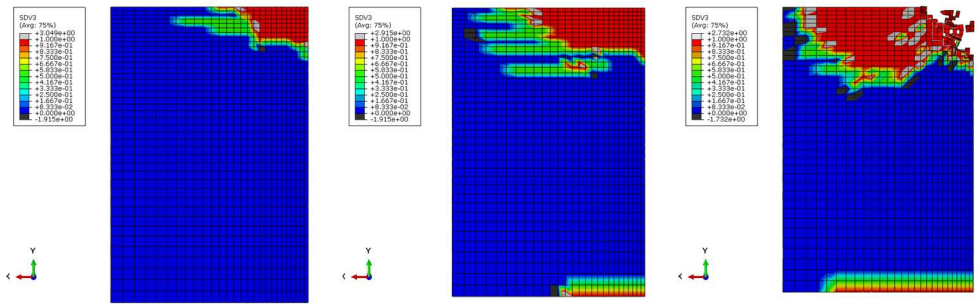

Figure 4 – Impact bottom layer matrix damage generated for initial velocities of 95 km/h (3 J), 227 km/h (17 J) and 550 km/h (100 J).

3.3 Model 1: Cross-Ply Layups $[0/90]_{2NS}$

Three-dimensional model meshes with a total of 35,424 hexahedral elements were developed. However, thick and thin ply meshes differ in the number of nodes due to their different number of inter-ply connections: 47,364 nodes for the thick ply model and 75,588 nodes for the thin ply model. In order to reduce the computational time, two planes of symmetry, XZ and YZ, were applied. A 3J energy impact of a rigid sphere, using iced water density in order to simulate a hail impact was replicated in both models. Comparing the generated damage with no perforation, it is possible to verify the ply thickness influence in the results.

Figure 5 shows comparisons for the behavior of thick and thin ply laminates during the impact. The sphere displacement and velocity, the kinetic energy, and the mean contact force between the sphere and the top layer were plotted as function of time. It can be seen, comparing the impact behavior of both models, that the thin model tends to be stiffer considering the sphere displacement and velocity. However, the thin ply laminate appears to slow down the process of energy return to the sphere after the peak, resulting in a lower energy absorbed level at the end of the impact process, which indicates a lower level of damage as compared to the thick ply laminate. This behavior can also be verified in the mean contact force vs. time plot with higher level of contact forces during this period.

Notice that, since the model presented herein is a model with two symmetry planes, only a quarter of the plate is shown in the figures bellow. The planes of symmetry are placed in top and left borders, the impact point being the upper left end, and the support constraints applied to the bottom and right.

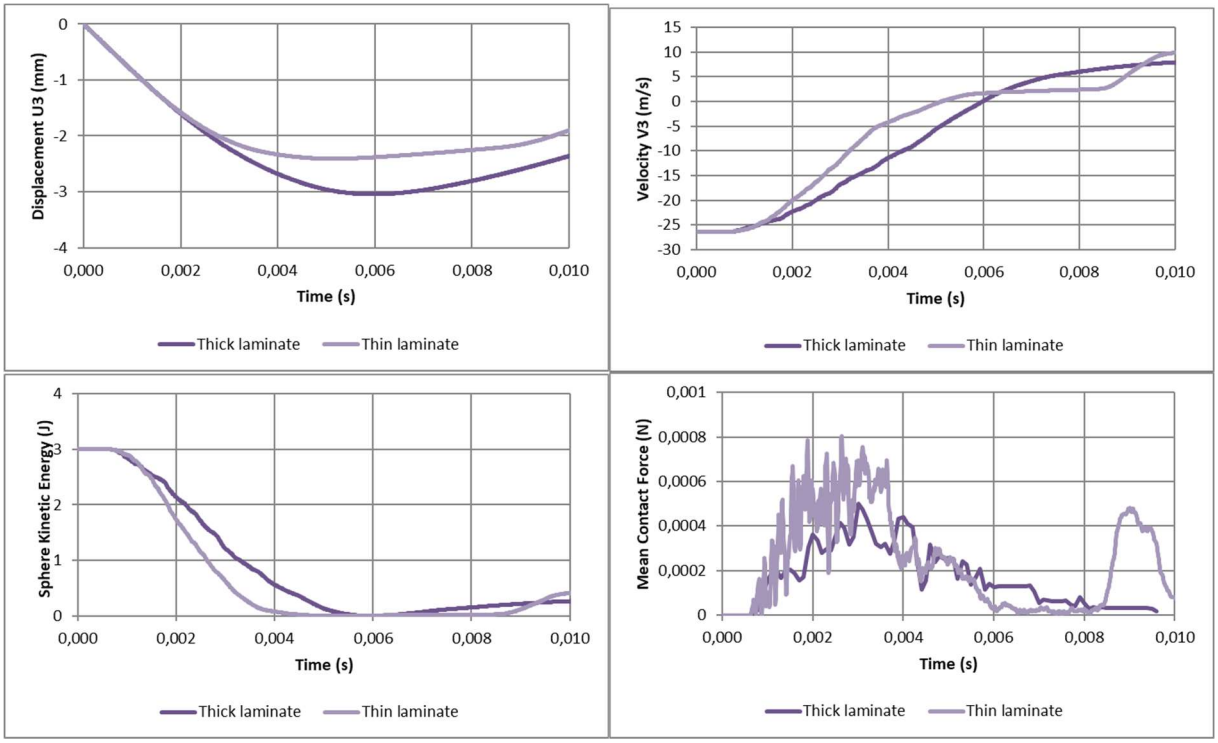

Figure 5 – 3J impact simulations results as functions of time for the sphere displacement (top left) and velocity (top right), the kinetic energy (bottom left), and the mean contact pressure between the sphere and the top layer (bottom right).

Figures 6 and 7 presents results of Hashin damage evaluation for both models. The most critical failure occurred due to transverse tensile stresses at the 0º ply in the laminate back (opposite) side of the impact. In Figure 6, ply #8 for the thick ply laminate (left) and ply #32 for the thin ply laminate (right) transverse tensile damage results were plotted for comparison. It can be seen that the damaged area for the thin ply laminate is smaller than the one for the thick ply laminate corroborating the impact energy absorption verified in Figure 4.

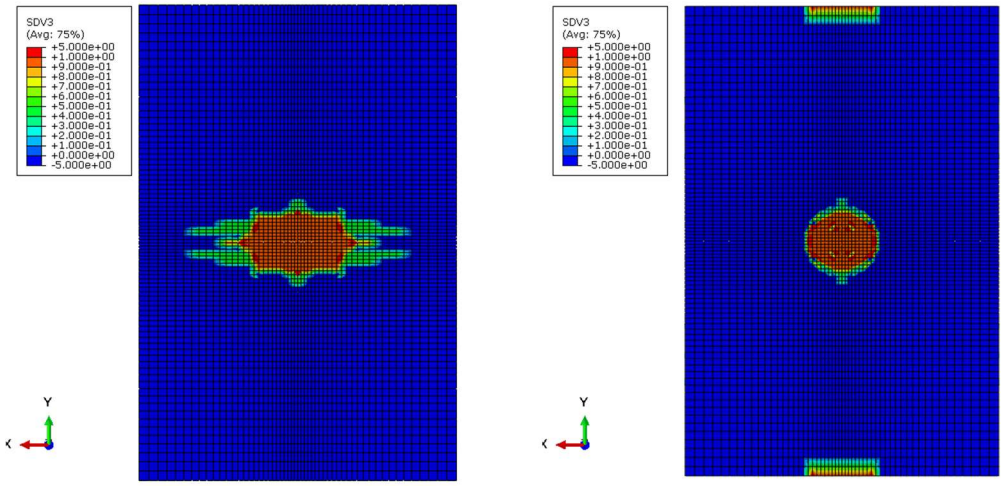

Figure 6 – Effect of 3J impact according to Hashin criterion: transverse tensile damage for ply #8 thick ply model (left) and ply #32 thin ply model (right).

In Figure 7, ply #1 for the thick ply laminate (left) and ply #1 for the thin ply laminate (right) longitudinal compressive damage results were plotted for comparison.

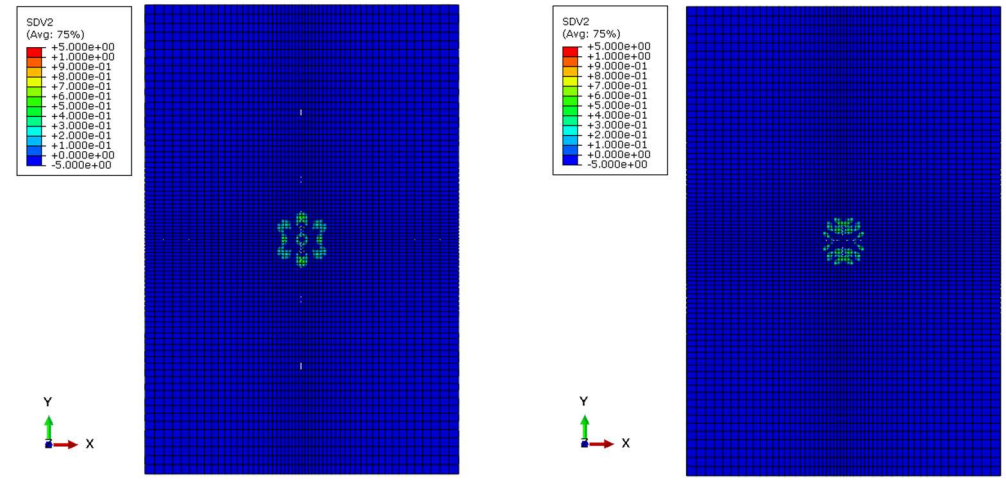

Figure 7 – Effect of 3J impact according to Hashin criterion: longitudinal compressive damage for ply #1 thick ply model (left) and ply #1 thin ply model (right).

Figure 8 shows, for a 17 J impact, comparisons for the behavior of thick and thin ply laminates during the impact. The sphere displacement and velocity, the kinetic energy, and the mean contact force between the sphere and the top layer were plotted as function of time. Again, comparing the impact behavior of both models, the thin model tends to be stiffer considering the sphere displacement and velocity. The thin ply laminate appears to slow down the process of energy return to the sphere after the peak, resulting in a lower energy absorbed level at the end of the impact process, which indicates a lower level of damage as compared to the thick ply laminate and, again, this behavior can also be verified in the mean contact force vs. time plot with higher level of contact forces during this period.

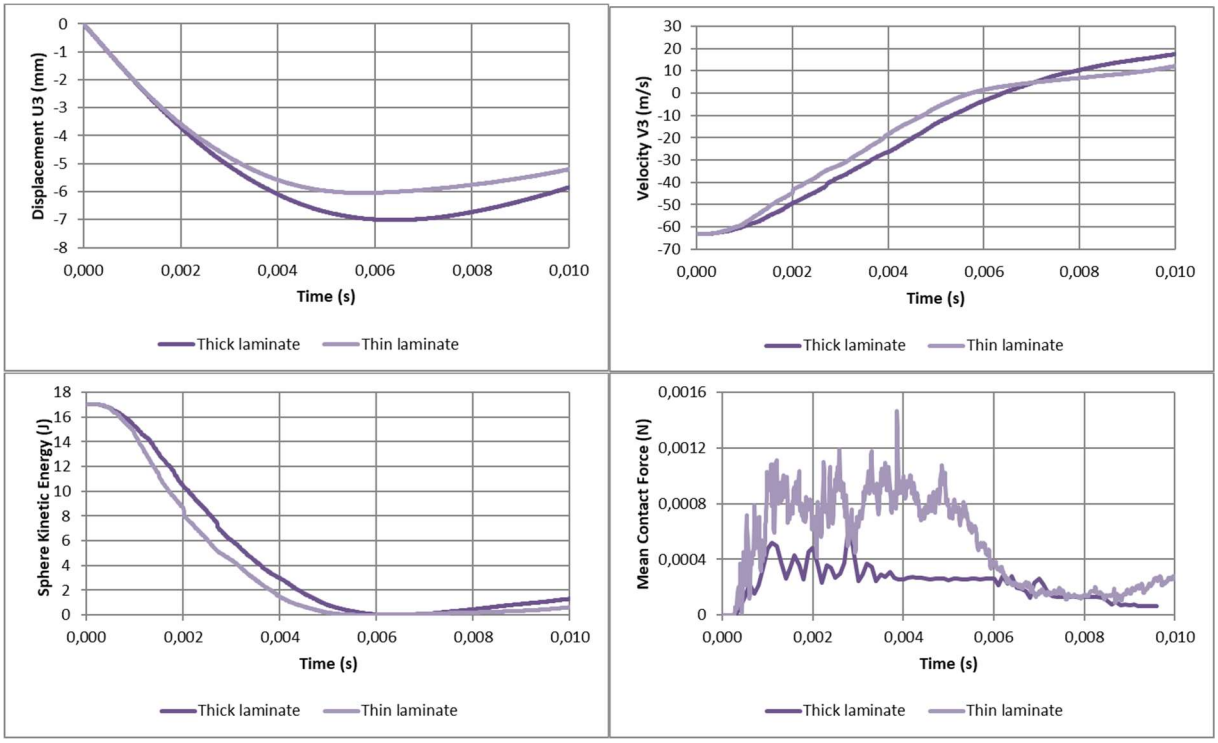

Figure 8 – 17J impact simulations results as functions of time for the sphere displacement (top left) and velocity (top right), the kinetic energy (bottom left), and the mean contact pressure between the sphere and the top layer (bottom right).

Figure 9 shows, for the 17 J energy level, results of Hashin damage evaluation for both models. Besides the increased most critical failure, they occur, as in the original case, due to transverse tensile stresses at the 0º ply in the laminate back (opposite) side of the impact and in the same laminae of the previous results. Again, it can be seen that the main damaged area for the thin ply laminate is more concentrated than the one for the thick ply laminate. On the other hand, it is possible to verify as a drawback a higher level of border damage in the thin ply case.

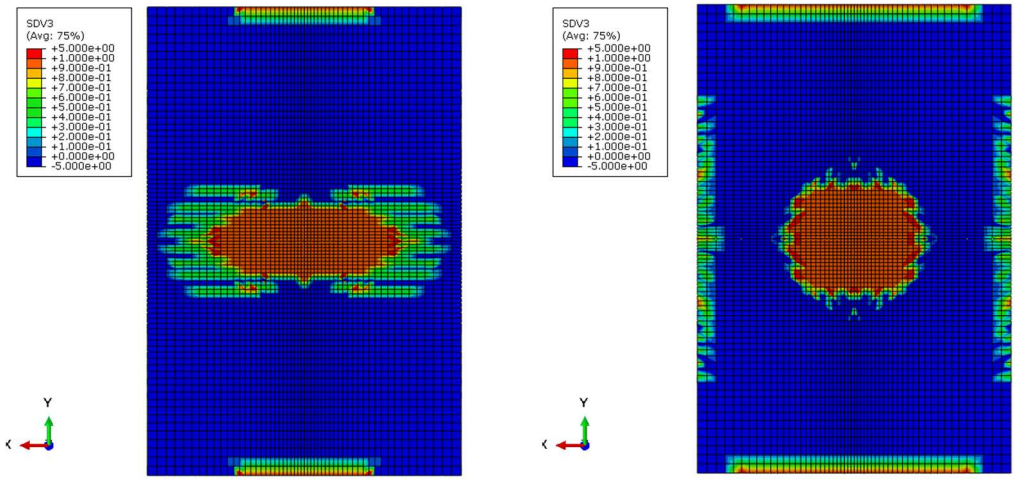

Figure 9 – Effect of 17J impact according to Hashin criterion: transverse tensile damage for ply #8 thick ply model (left) and ply #32 thin ply model (right).

In Figure 10, ply #1 for the thick ply laminate (left) and ply #1 for the thin ply laminate (right), again the same plies of the previous case, it can be seen a similar longitudinal compressive damage results presented for thick and thin plies cases.

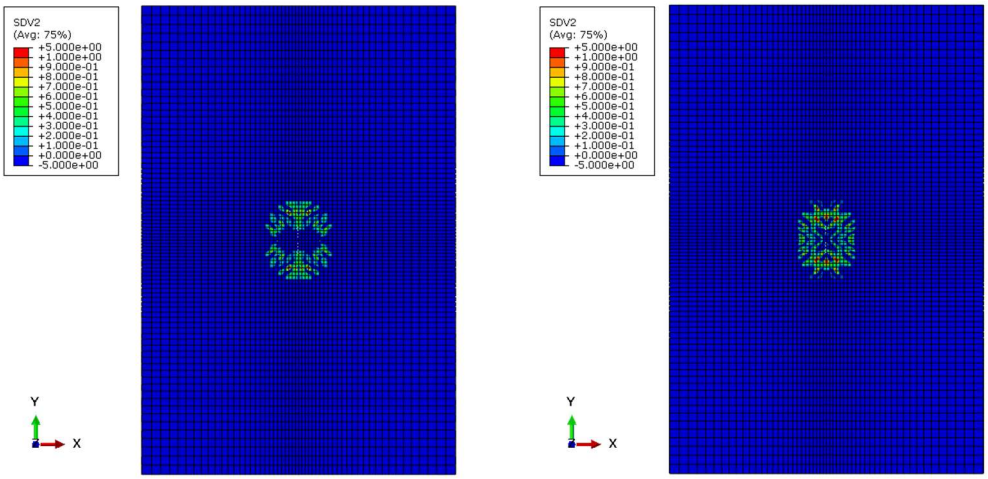

Figure 10 – Effect of 17J impact according to Hashin criterion: longitudinal compressive damage for ply #1 thick ply model (left) and ply #1 thin ply model (right).

3.4 Model 2: Quasi-Isotropic Layups $[+45/0/-45/90]_{NS}$

In this subsection, due to the quasi-isotropic layups caracteristics, the planes of symmetry, XZ and YZ, were not applied. So, the correspondent complete three-dimensional model meshes, with a total of 148,513 hexahedral elements, were developed. However, thick and thin ply meshes still differ in the number of nodes due to their different number of inter-ply connections: 186,838 nodes for the thick ply model and 298,390 nodes for the thin ply model. Again, a 3J and a 17J energy impact of a rigid sphere, using iced water density in order to simulate a hail impact was replicated in both models. Comparing the generated damage with no perforation, it is possible to verify the ply thickness influence in the results.

Figures 11 and 12 presents results of Hashin damage evaluation for both quasi-isotropic complete models. In Figure 11 it can be seen the most critical failure occurred due to transverse tensile stresses at the 0º ply in the laminate back (opposite) side of the impact. In Figure 9, ply #8 for the thick ply laminate (left) and ply #32 for the thin ply laminate (right) transverse tensile damage results were plotted for comparison.

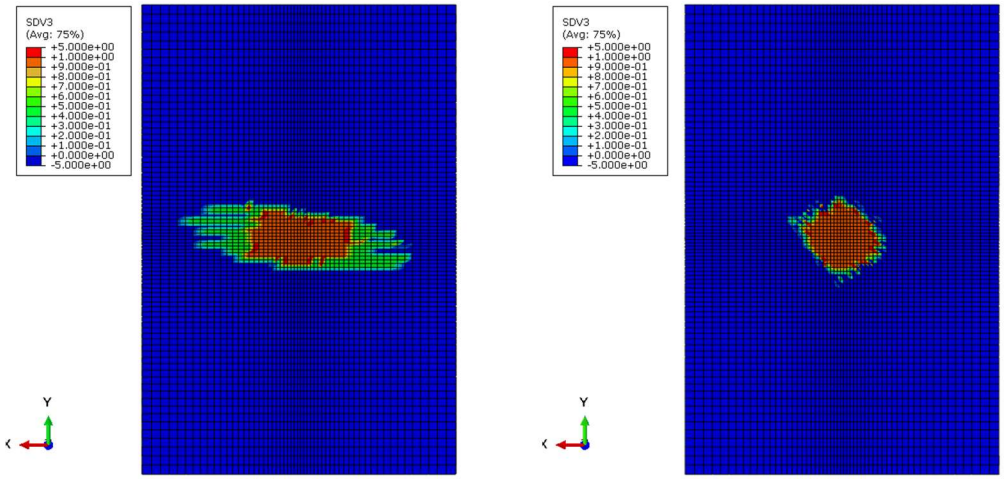

Figure 11 – Effect of 3J impact according to Hashin criterion: transverse tensile damage for ply #8 thick ply model (left) and ply #32 thin ply model (right).

In Figure 12, for ply #8 for the thick ply laminate (left) and ply #32 for the thin ply laminate (right), is shown the most critical failure occurred due to transverse tensile stresses at the 0° ply in the laminate back (opposite) side of the impact, it can be seen that the main damaged area for the thin ply laminate is more concentrated than the one for the thick ply laminate. Notice that, using a quasi-isotropic layup, it is possible to avoid the border damage effect in both thick and thin ply cases.

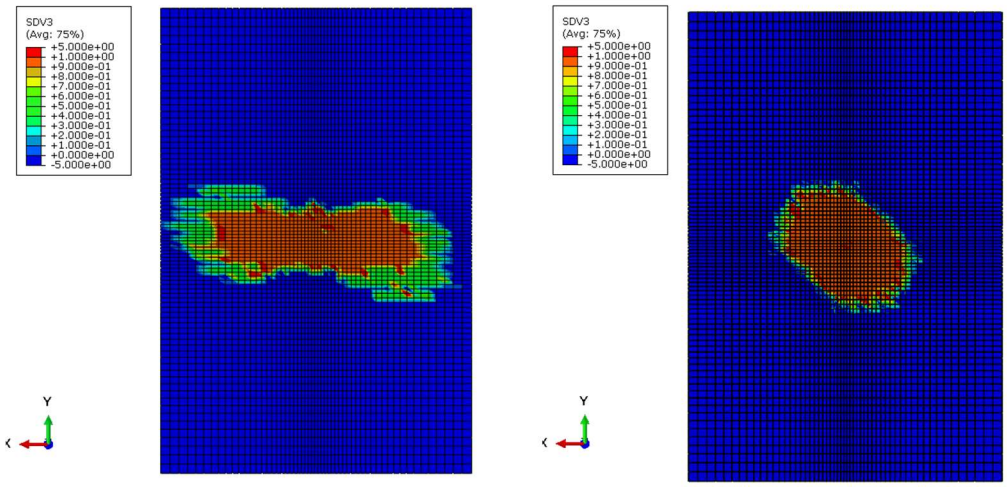

Figure 12 – Effect of 17J impact according to Hashin criterion: longitudinal compressive damage for ply #8 thick ply model (left) and ply #32 thin ply model (right).

4 CONCLUSIONS

Analyzing the simulation results for the impact damage generated in the laminate presented in this work, besides that the damage can't be entirely avoided, it is usefull to understand the mechanical behavior of the material and the modification of this behavior due to rearrangement of plies. Complex test programs are necessary to fully characterize the material and the failure modes in order to develop accurate numerical methods, however, based in this study is possible to evaluate the effects of damage generated due to low velocity impact in carbon/epoxy composite laminates, so that further predictions can be made for after impact loading schemes, such as compression after impact (CAI), tension after impact (TAI), and shear after impact (ShAI). Based on the above results it is possible foresee a reduction of expected damage as a reduction in ply thickness influence, so using more plies and the same amount of material, on the impact damage in carbon/epoxy composite. This behavior corroborates with the expectation of lower probability of occurrence of microcracks. On the other hand, the use of thinner plies may increase the costs of manufacturing and, at some point, even be impossible to manufacture.

ACKNOWLEDGEMENTS

The authors are thankful for the assistance of the Structural Engineering Department of UFMG and the Department of Mechanical Engineering of Hanyang University. This work was supported by CAPES, CNPq, and FAPEMIG.

REFERENCES

[1] W. J Cantwell and J. Morton, The impact resistance of composite materials – a review, *Composites*, **22**, 1991, pp. 347-362. (doi: 10.1016/0010-4361(91)90549-V)

[2] M.O.W. Richardson and M.J. Wisheart, Review of low-velocity impact properties of composite materials, *Composites Part A*, **27A**, 1996, pp. 1123-1131. (doi: 10.1016/1359-835X(96)00074-7)

[3] D.J. Elder, R.S. Thomson, M.Q. Nguyen and M.L. Scott, Review of delamination predictive methods for low speed impact of composite laminates, *Composite Structures*, **66**, pp. 677-683, 2004. (doi: 10.1016/j.compstruct.2004.06.004)

[4] G.A.O. Davies and X. Zhang, Impact damage prediction in carbon composite structures, *International Journal of Impact Engineering*, **16**, 1994, pp. 149-170. (doi: 10.1016/0734-743X(94)00039-Y)

[5] A.P. Christoforou and A.S. Yigit, Scaling of low-velocity impact response in composite structures, *Composite Structures*, **91**, 2009, pp. 358-365. (doi: 10.1016/j.compstruct.2009.06.002)

[6] R. Tiberkak, M. Bachene, S. Rechak and B. Necib, Damage prediction in composite plates subjected to low velocity impact, *Composite Structures*, **83**, 2008, pp. 73-82. (doi: 10.1016/j.compstruct.2007.03.007)

[7] J.P. Hou, N. Petrinic, C. Ruiz and S.R. Hallett, Prediction of impact damage in composite plates, *Composites Science and Technology*, **60**, 2000, pp. 273-281. (doi: 0.1016/S0266-3538(99)00126-8)

[8] G.A. Schoeppner and S. Abrate, Delamination threshold loads for low velocity impact on composite laminates, *Composites Part A*, **31**, 2000, pp. 903-915. (doi: 10.1016/S1359-835X(00)00061-0)

[9] J.P. Hou, N. Petrinic, C. Ruiz, A delamination criterion for laminated composites under low-velocity impact, *Composites Science and Technology*, **61**, 2001, pp. 2069-2074. (doi: 10.1016/S0266-3538(01)00128-2)

[10] F. Aymerich, G. Lecca and P. Priolo, Modelling of delamination growth in composite laminates by the virtual internal bond method, *Composites: Part A*, **39**, 2008, pp. 145-153. (doi: 10.1016/j.compositesa.2007.11.012)

[11] S. Abrate, Modeling of impacts on composite structures, *Composite Structures* **51**, 2001, pp. 129-138. (doi: 10.1016/S0263-8223(00)00138-0)

[12] A.P. Christoforou, Impact dynamics and damage in composite structures, *Composite Structures* **52**, 2001, pp. 181-188. (doi: 10.1016/S0263-8223(00)00166-5)

[13] R. Borg, L. Nilsson and K. Simonsson, Simulation of low velocity impact on fiber laminates using a cohesive zone based delamination model, *Composites Science and Technology*, **64**, 2004, pp. 279-288. (doi: 10.1016/S0266-3538(03)00256-2)

[14] F. Aymerich, F. Dore and P. Priolo, Prediction of impact-induced delamination in cross-ply composite laminates using cohesive interface elements, *Composites Science and Technology*, **68**, 2008, pp. 2383-2390. (doi: 10.1016/j.compscitech.2007.06.015)

[15] ASTM D7137/D7137M-12, *Standard test method for compressive residual strength properties of damaged polymer matrix composite plates*, ASTM International, West Conshohocken, PA, USA, 2012.

[16] Daniel, I.M., and Ishai, O. "*Engineering Mechanics of Composite Materials*." 1 ed. Oxford University Press. 1994.

[17] Z. Hashin, Failure Criteria for Unidirectional Fiber Composites, *Journal of Applied Mechanics*, **47**, 1980, pp. 329-334. (doi: 10.1016/j.compscitech.2007.06.015)

[18] Z. Hashin and A. Rotem, "*A Fatigue Criterion for Fiber-Reinforced Materials*," *Journal of Composite Materials*, **7**, 1973, pp. 448-464. (doi: 10.1016/j.compscitech.2007.06.015)